MCB Accepts, published online ahead of print on 28 July 2014
Mol. Cell. Biol. doi:10.1128/MCB.00287-14

Absence of a red blood cell phenotype in mice with hematopoietic deficiency of SEC23B

Running title: Hematopoietic SEC23B deficiency

Rami Khoriaty[1]*, Matthew P. Vasievich[2]*, Morgan Jones[3], Lesley Everett[2], Jennifer Chase[3], Jiayi Tao[4], David Siemieniak[3], Bin Zhang[4], Ivan Maillard[1,3], David Ginsburg[1,2,3,5,6]#

[1]Department of Internal Medicine, University of Michigan, Ann Arbor, MI; [2]Department of Human Genetics, University of Michigan Medical School, Ann Arbor, MI; [3]Life Sciences Institute, University of Michigan, Ann Arbor, MI; [4]Genomic Medicine Institute, Cleveland Clinic Lerner Research Institute, Cleveland, OH; [5]Department of Pediatrics and Communicable Diseases, University of Michigan, Ann Arbor, MI; [6]Howard Hughes Medical Institute, University of Michigan, Ann Arbor, MI

Matt Vasievich's current address: Department of Dermatology, Cleveland Clinic, Cleveland, OH.

Jiayi Tao's current address: Case Western Reserve University, Cleveland, OH

Corresponding author:

Email: ginsburg@umich.edu

Phone: 734-647-4808

Fax: 734-936-2888

* Authorship note: Rami Khoriaty and Matt P. Vasievich contributed equally to the work.

Abstract word count: 196

Article length for abstract, introduction, results, discussion, and figure legends: 28,079 characters (excluding spaces).

Word count for the Materials and Methods section: 1,659.

Combined word count for the Introduction, Results, and Discussion sections: 2,810.

Abstract

Congenital dyserythropoietic anemia type II (CDAII) is an autosomal recessive disease of ineffective erythropoiesis characterized by increased bi/multi-nucleated erythroid precursors in the bone marrow. CDAII results from mutations in *SEC23B*. The SEC23 protein is a core component of the coat protein complex II-coated vesicles, which transport secretory proteins from the endoplasmic reticulum to the Golgi apparatus. Though the genetic defect underlying CDAII has been identified, the pathophysiology of this disease remains unknown. We previously reported that SEC23B-deficient mice die perinatally, exhibiting massive pancreatic degeneration, with this early mortality limiting evaluation of the adult hematopoietic compartment. We now report that mice with SEC23B-deficiency restricted to the hematopoietic compartment survive normally and do not exhibit anemia or other CDAII characteristics. We also demonstrate that SEC23B-deficient hematopoietic stem cells (HSC) do not exhibit a disadvantage at reconstituting hematopoiesis when compared directly to wild type HSC in a competitive repopulation assay. Secondary bone marrow transplants demonstrated continued equivalence of SEC23B-deficient and WT HSC in their hematopoietic reconstitution potential. The surprising discordance in phenotypes between SEC23B-deficient mice and humans may reflect an evolutionary shift in SEC23 paralog function and/or expression, or a change in a specific COPII cargo critical for erythropoiesis.

Introduction

Congenital dyserythropoietic anemia type II (CDAII), also known as Hereditary Erythroblastic Multinuclearity with a Positive Acidified-Serum lysis test (HEMPAS), is an autosomal recessive disease characterized clinically by mild to moderate anemia resulting from ineffective erythropoiesis (median hemoglobin 9.1-9.8 g/dL), the presence of bi-/multi-nucleated erythroblasts in the bone marrow (BM), jaundice from indirect hyperbilirubinemia, and splenomegaly (1, 2). CDAII is distinguished from other congenital anemias by a characteristic double membrane appearance on red blood cell (RBC) electron microscopy resulting from residual endoplasmic reticulum (ER) (3), a faster migrating and narrower band on SDS-PAGE for the RBC membrane protein band 3, and lysis of RBCs in some, but not all, acidified normal sera (Ham's test) (1, 2).

CDAII results from homozygous or compound heterozygous mutations in *SEC23B* (4), one of the two mammalian paralogs of *SEC23*. SEC23 is a core component of the coat protein complex II (COPII)-coated vesicles that transport cargo proteins from the ER to the Golgi apparatus (2, 5). More than 60 different *SEC23B* mutations have been identified in CDAII patients (4, 6-14), affecting every domain of the protein (7). No patient with two nonsense *SEC23B* mutations has been reported, suggesting that complete loss of SEC23B may be lethal. Homozygosity for specific missense mutations in *SEC23A*, the paralog of *SEC23B*, results in cranio-lenticulo-sutural-dysplasia (15), thought to be due to defective collagen secretion.

Despite the identification of the genetic defect, the molecular mechanism by which deficiency of SEC23B results in the CDAII phenotype remains unknown (2). Nearly all

proteins destined for secretion from the cell or export to the cell membrane or lysosome (~1/3 of the mammalian proteome) are dependent on COPII vesicles for transport from the ER to Golgi. Thus, it is surprising that deficiency of a key, ubiquitously expressed component of the COPII coat, SEC23B, results in a phenotype apparently restricted to the red blood cell. Reports of curative allogeneic bone marrow transplantation for CDAII suggest that the mechanism responsible for the erythroid defect is intrinsic to the hematopoietic compartment (9, 16, 17).

We previously reported that mice homozygous for a *Sec23b* gene-trap allele (*Sec23b*$^{gt/gt}$) die within 24 hours of birth, exhibiting degeneration of the pancreas and other professional secretory tissues (18). The perinatal lethality precluded assessment of adult hematopoietic function in these mice. We now report that chimeric mice with SEC23B-deficiency restricted to the hematopoietic compartment can support the normal production of adult RBCs, with no apparent abnormality in hematopoiesis. Competitive hematopoietic stem cell (HSC) transplantation assays also fail to demonstrate a disadvantage of *Sec23b*$^{gt/gt}$ HSC at reconstituting hematopoiesis compared to WT HSC.

Materials and Methods

Generation of SEC23B-deficient mice

Two *Sec23b* mutant mouse lines, one with a gene-trap (gt) cassette insertion into *Sec23b* intron 19 ($Sec23b^{gt}$), and the second with a conditional gt insertion in *Sec23b* intron 4 ($Sec23b^{cgt}$), were generated as previously described (Fig. 1A and B) (18). All $Sec23b^{gt}$ mice used in this study were generated from heterozygous mice backcrossed to C57BL/6J mice for > 10 generations. The $Sec23b^{cgt}$ allele was derived from C57BL/6J ES cells (18), and maintained on a pure background by backcrosses exclusively to C57BL/6J. $Sec23b^{cgt/+}$ mice were crossed to a mouse ubiquitously expressing FLPe under the control of the human *β-actin* promoter (β-actin FLP) (Jackson laboratory stock # 005703) to excise the gt cassette and generate the *Sec23b* floxed allele ($Sec23b^{fl}$), with exons 5 and 6 flanked by *loxP* sites (Fig. 1B). Mice with complete deficiency of SEC23B ($Sec23b^{-}$) were generated by crossing the $Sec23b^{fl}$ allele to a mouse expressing Cre recombinase driven by an EIIA promoter (EIIA Cre) (Jackson laboratory stock # 003724). Deletion of *Sec23b* exons 5 and 6 results in a frameshift and downstream stop codon in exon 7. Mice were housed at the University of Michigan and all procedures were in accordance with the regulations of the Animal Care and Use Committee.

PCR genotyping

Genotyping for the $Sec23b^{gt}$ allele was performed as previously described (18). The $Sec23b^{cgt}$ allele was genotyped by a three-primer polymerase chain reaction (PCR) assay using a forward primer (F1) located in *Sec23b* intron 4 upstream of the insertion

site and two reverse primers, one (cgtB1) located in the gene-trap insertion cassette between the two FRT sites and the second (cgtR1) located in intron 4 downstream of the FRT sites. This PCR reaction results in a 475 base pair (bp) product from the wild type (WT) allele (F1:cgtR1) and a 344 bp product from the Sec23b^{cgt} allele (F1:cgtB1), which are resolved on 2% (weight/volume) agarose gel electrophoresis (Fig. 1C). Genotyping for the *Sec23b^{fl}* and *Sec23b^{-}* alleles was performed with a three-primer competitive PCR assay consisting of the forward primer F1, a second forward primer (F2) located in intron 6 between the two *loxP* sites, and a common reverse primer (R1) located in intron 6 downstream of the insertion site. This reaction produces a 235 bp product from the WT allele (F2:R1), a 269 bp product from the *Sec23b^{fl}* allele (F2:R1), and a 336 base pair product from the *Sec23b^{-}* allele (F1:R1), which are resolved by 3% agarose gel electrophoresis (Fig. 1D). Locations of the genotyping primers are indicated in figures 1A and 1B. Primer sequences are shown in Table 1.

Fetal liver cell (FLC) transplants

Timed matings were performed by intercrossing *Sec23b$^{+/gt}$* mice or *Sec23b$^{+/-}$* mice. The following morning, designated as E0.5, matings were separated. Pregnant female mice were euthanized at E17.5 post-coitus. Recovered fetuses were separated and placed individually in Petri dishes on ice under sterile conditions. A tail biopsy was obtained from each fetus for genotyping. Fetal livers were individually disrupted and dispersed cells were suspended in RPMI 1640 (Gibco) supplemented with 2% fetal bovine serum (FBS) at 4°C. FLC were washed twice in RPMI 1640 + 2% FBS, and then suspended in 65% RPMI 1640, 25% FBS, and 10% DMSO, frozen at -80°C overnight, and stored in vapor phase liquid nitrogen at -186°C.

Six to twelve week old C57BL/6J recipient mice were lethally irradiated with two doses of 550 rads separated by 3 hours in a Cs Gammacell 40 Exactor irradiator (MDS Nordion). Three hours following completion of irradiation, frozen WT and SEC23B-deficient FLC (*Sec23b*$^{gt/gt}$ or *Sec23b*$^{+/-}$ FLC) were thawed in a 37°C water bath. 10^6 cells were suspended in 300 μl RPMI 1640 with 2% FBS and injected into the retro-orbital venous sinus of recipient mice. For each transplant experiment, control mice were injected with media only. No control mice survived beyond 12 days. Transplanted mice were provided with acidified water (pH = 2.35) for 3 weeks post-transplantation.

Competitive FLC transplants

C57BL/6J mice expressing high levels of green fluorescent protein (GFP) in all tissues including hematopoietic cells (19) (under the control of the human ubiquitin C promoter (UBC-GFP mice)) were obtained from the Jackson Laboratory (stock # 004353). FLC from crosses between male mice homozygous for the UBC-GFP transgene (UBC-GFP$^{tg/tg}$) and female C57BL/6J mice were harvested at day 17.5 post-coitus and stored as described above. UBC-GFP$^{tg/+}$ FLC were mixed in a 1:1 ratio with either *Sec23b*$^{gt/gt}$ FLC (experimental arm) or WT FLC (control arm) and transplanted into lethally irradiated C57BL/6J recipients as described above.

Bone marrow cells were isolated from the hind limbs of each chimeric mouse. The number of GFP(-) cells per 2 hind limbs was calculated for each hematopoietic lineage by multiplying the ratio of GFP(-)/GFP(+) cells in each lineage by the total number of cells per lineage. The number of GFP(-) cells per two hind limbs should be proportional

148 to the contribution of GFP(-) cells to each lineage, corresponding to *Sec23b*$^{gt/gt}$ cells in
149 the experimental arm and WT cells in the control arm.

150 GFP(-) mature myeloid cells (Mac1+ Gr1+) were FACS sorted from bone marrows
151 harvested from chimeric recipient mice. Myeloid cells were genotyped for *Sec23b*.

152 For secondary transplants, whole BM cells were harvested from these chimeric recipient
153 mice twenty weeks after the competitive FLC transplant, and 2 x 10^6 cells were
154 transplanted into lethally irradiated secondary C57BL/6J recipients.

155 **Complete blood counts (CBC) and BM analysis**

156 Twenty microliters of blood were drawn from the retro-orbital venous sinuses of mice
157 anesthetized with isoflurane. Blood was diluted 1:10 in 5% Bovine Serum Albumin
158 (BSA) in Phosphate Buffered Saline (PBS) pH 7.4. CBC were performed on the
159 Advia120 whole blood analyzer (Siemens) according to the manufacturer's instructions.

160 Following pentobarbital-induced anesthesia, BM was flushed from femurs and tibias of
161 each mouse using either Hank's balanced salt solution (Gibco) or RPMI 1640,
162 supplemented with 5% FBS. BM cells were used for flow cytometry (below) and a
163 subset (~ 160,000 cells) was collected by centrifugation in a cytospin (Thermo scientific
164 cytospin 4 cytocentrifuge), stained with the HEMA 3 kit (Fisher), and examined under
165 light microscopy. BM cytospins were evaluated by an investigator blinded to mouse
166 genotype.

167 **Flow cytometry**

Peripheral blood or BM single cell suspensions were incubated with various antibodies. The following antibodies were obtained from BioLegend, eBiosciences, or BD Biosciences: anti-Ter119, Gr1 (RB6-8C5), Mac1 (M1/70), CD3 (145-2C11), CD16/CD32 (2.4G2), CD45R/B220 (RA3-6B2), CD150 (TC15-12F12.2), Sca1 (D7), CD117 (2B8), CD48 (BCM1), CD19 (6D5), TCRβ (H57-597), CD8 (53-6.7), CD11c (N418), CD4 (RM4-4), NK1.1 (PK136), and TCRγ/δ (GL3). The following antibody cocktail was used to exclude lineage positive (Lin+) cells: anti-Ter119, CD11b, CD11c, Gr1, C220, CD19, CD3, TCRβ, TCRγ/δ, CD8, and NK1.1. Stained cells were analyzed by flow cytometry using flow cytometers FACSCanto II, FACSAria II, or FACSAria III (Becton Dickinson Biosciences). Dead cells were excluded with DAPI where appropriate (Sigma). Files were analyzed with FlowJo (Tree Star).

Cell sorting

Ter119+ erythroid precursors were sorted from reconstituted bone marrows of recipient mice using FACSAria II. Ter119+ erythroid precursors were also purified from E17.5 FLC. Mononuclear cells prepared from E17.5 livers were incubated with APC-conjugated anti-Ter119+ antibody (Biolegend) for 30 minutes on ice, washed twice with PBS containing 4% FBS, and then treated with anti-APC conjugated magnetic beads (Miltenyi biotech) for 15 minutes. Cells were then washed once and suspended in PBS + 4% FBS. Ter119+ positive cells were collected using LS MACS separation columns (Miltenyi biotech) mounted on a magnet stand according to manufacturer's instructions.

RBC ghost preparation

Seventy microliters of peripheral blood were centrifuged at 2300 g. The pellet was washed twice with PBS (pH 7.4) and then lysed by suspension in ghost lysis buffer (5 mM Na2PO4, 1.3 mM EDTA, pH = 7.6) containing protease inhibitor (1 protease inhibitor tablet (Roche, stock # 11873580001) per 50 ml ghost lysis buffer). Lysates were centrifuged at 16,000 g and the supernatants containing the RBC membrane fraction were collected and washed 4-6 times in ghost lysis buffer. RBC ghosts were stored at -80°C in lysis buffer.

Electron microscopy

Cells were fixed in 2.5% glutaraldehyde in 0.1M Sorensen's buffer (pH 7.4) overnight at 4°C. After 2 rinses with 10-20 milliliters of Sorensen's buffer, cells were fixed with 1% osmium tetroxide in 0.1M Sorensen's buffer, rinsed in double distilled water, and then *en bloc* stained with aqueous 3% uranyl acetate for 1 hour. Cells were dehydrated in ascending concentrations of ethanol, rinsed twice in 100% ethanol, and embedded in epoxy resin. Samples were ultra-thin sectioned at 70 nm in thickness and stained with uranyl acetate and lead citrate. Sections were examined on a Philips CM100 electron microscope at 60kV. Images were recorded digitally using a Hamamatsu ORCA-HR digital camera system operated with AMT software (Advanced Microscopy Techniques Corp., Danvers, MA).

Western blot

Proteins were separated by SDS gel electrophoresis using 4-20% tris-glycine gels (Invitrogen) and tris-glycine running buffer or using 4-12% Bis-Tris gels (Invitrogen) and MOPS running buffer (Invirogen). Proteins were then transferred onto nitrocellulose

membranes (BioRad). For X-ray development, membranes were blocked in 5% milk/TBST (weight/volume), probed with primary antibody, washed 3 times in TBST, probed with peroxidase coupled secondary antibodies (Thermo Scientific), washed 3 times in TBST, and developed using Western Lightning Plus-ECL (Perkin-Elmer). Quantitative western blots were performed using Odyssey (LICOR Biosciences) according to the manufacturer's instructions. Secondary antibodies utilized were IRDye 680RD or IRDye 800 CW. Band intensities were quantified using the Odyssey software. SEC23A band intensity was normalized to beta-actin or RalA.

Antibodies

Anti-SEC23B and anti-SEC23A antibodies were generated in rabbit against peptides LTKSAMPVQQARPAQPQEQP and DNAKYVKKGTKHFEA respectively. Anti-Band3 and anti-GAPDH antibodies were obtained from Millipore. Anti-actin antibody was obtained from Santa Cruz.

qRT-PCR

RNA was isolated with Trizol. Reverse transcription was performed using the Superscript First-Strand Synthesis System for RT-PCR (Invitrogen) with random primers. Real-time PCR amplification was performed in triplicates with Power SYBR Green PCR Master Mix (Applied Biosystems) using the Applied Biosystems 7900HT Fast real-time PCR System. Relative gene expression was calculated using the $2^{-\Delta\Delta CT}$ method. Beta-actin or GAPDH were used as internal controls. Two samples of each genotype were analyzed, each in triplicate. qPCR primer sequences are listed in table 1.

Results

Transplantation of SEC23B-deficient HSC does not result in a CDAII phenotype

SEC23B deficient mice die perinatally, exhibiting degeneration of their professional secretory tissues but no evidence of anemia at birth (18). To assess the impact of SEC23B-deficiency on adult mouse hematopoietic function, equal numbers of FLC collected from either *Sec23b*$^{gt/gt}$ or WT E17.5 embryos were transplanted into lethally irradiated C57BL/6J recipient mice. Livers harvested from *Sec23b*$^{gt/gt}$ and WT E17.5 embryos exhibited no significant differences in total cell counts or numbers of long-term HSCs (ckit+ Sca1+ CD48- CD150+ Lin-) (20) measured by flow cytometry (Fig. 2A, B, and C). Hemoglobin (Fig. 3A) and hematocrit (Fig. 3B) levels measured at weeks 6, 8, 12, and 25 post-transplantation were all the within the normal range and indistinguishable between mice transplanted with *Sec23b*$^{gt/gt}$ FLC and recipients of WT FLC, as were spleen weights (Fig. 3C) and bone marrow myeloid to erythroid ratios (Fig. 3D). There was also no increase in the number of bi/multi-nucleated RBC precursors observed in the recipients of *Sec23b*$^{gt/gt}$ BM (Fig. 3E).

Characteristic RBC abnormalities in humans with CDAII include a “double membrane” appearance on transmission electron microscopy, and narrower band size together with a shift in the mobility of membrane protein band 3 on sodium dodecylsulfate-polyacrylamide gel electrophoresis. RBC from mice transplanted with *Sec23b*$^{gt/gt}$ FLCs did not exhibit either of these abnormalities (Fig. 4A-C).

SEC23B deficient FLC and WT FLC are equivalent in reconstituting erythropoiesis

To assess for a more subtle hematopoietic defect, SEC23B deficient FLC were tested for their ability to reconstitute hematopoiesis as compared to WT FLC in a competitive repopulation assay. In this experiment, *Sec23b*$^{gt/gt}$ FLC were mixed with UBC-GFP$^{tg/+}$ *Sec23b*$^{+/+}$ FLC in a 1:1 ratio and co-transplanted into lethally irradiated C57BL/6J recipient mice. Following engraftment, hematopoietic cells from recipient mice were characterized by GFP expression to distinguish cells of *Sec23b*$^{gt/gt}$ or WT FLC origin. Control mice were co-transplanted with a 1:1 ratio of WT FLCs cells with or without the UBC-GFP$^{tg/+}$ transgene.

Over the course of 18 weeks of follow-up, WT FLC exhibited no competitive advantage at reconstituting erythropoiesis compared to SEC23B-deficient FLC (Fig. 5A). Similarly, no defects were observed in the ability of *Sec23b*$^{gt/gt}$ FLC to differentiate into neutrophils (Fig. 6 A) or lymphocytes (Fig. 6B and C).

Eighteen weeks following transplantation, reconstituted bone marrows and thymi were harvested from transplant recipients and the relative contribution of *Sec23b*$^{gt/gt}$ and WT cells to each hematopoietic compartment was evaluated. Erythroid cells were stratified by forward scatter and CD71 expression to identify primitive progenitors (larger cells expressing higher levels of CD71), mature cells (smaller cells expressing low levels of CD71), and erythroid cells in intermediate stages of development (average or small size cells expressing high levels of CD71) (21). *Sec23b*$^{gt/gt}$ and WT cells contributed similarly to all populations of erythroid cells examined (Fig. 5B).

The contribution of GFP(-) *Sec23b*$^{gt/gt}$ cells to the populations of long-term HSC (Fig. 6D) and myeloid cells (Fig. 6E) in the BM, and to all subgroups of T-lymphocytes (Fig.

6F) in the thymus was equivalent to that of GFP(+) WT cells. There was a trend for some subsets of T-lymphocytes to be under-represented (*Sec23b*$^{gt/gt}$ CD8+ TCRβ immature single positive cells, CD4+ CD8+ double positive cells, and CD4+ T-lymphocytes); however, this did not reach statistical significance after correction for multiple observations. In contrast, BM *Sec23b*$^{gt/gt}$ B-lymphocytes (Fig. 6G) were under-represented relative to their WT counterparts ($p = 0.005$).

To exclude the possibility that the reconstituted GFP(-) hematopoietic cells in recipient mice were derived from host reconstitution rather than *Sec23b*$^{gt/gt}$ FLC, GFP(-) mature myeloid cells (Mac1+ Gr1+) were FACS sorted from bone marrows of mice co-transplanted with GFP(-) *Sec23b*$^{gt/gt}$ FLC and GFP(+) WT FLC. The genotype of the isolated myeloid cells was confirmed to be *Sec23b*$^{gt/gt}$ (Fig. 7).

SEC23B deficient HSC and WT HSC are equivalent in their hematopoietic reconstitution potential

To further test for the hematopoietic reconstitution potential of *Sec23b*$^{gt/gt}$ HSC, bone marrows chimeric for *Sec23b*$^{gt/gt}$ and WT HSC were harvested from the competitive FLC transplant recipients (described above) and transplanted into secondary WT recipients. Over the course of 18 weeks of follow-up, the contribution of *Sec23b*$^{gt/gt}$ and WT HSC to the reconstituted erythroid, myeloid, B-cell and T-cell compartments was equivalent (Fig. 8A, and Fig. 9A-C). Bone marrows from a subset of secondary transplant recipients were analyzed at 26 weeks post-transplantation. Persistence of GFP(-) *Sec23b*$^{gt/gt}$ erythroid cells in all stages of erythroid differentiation (Fig. 8B) and *Sec23b*$^{gt/gt}$ long-term HSC (Fig. 8C) was observed.

A second *Sec23b* null allele confirms the absence of a RBC phenotype in SEC23B-deficient mice

Sec23b$^{gt/gt}$ murine embryonal fibroblasts express a SEC23B/βGEO fusion protein resulting from the gene-trap insertion into intron 19 of *Sec23b*. Though SEC23B/βGEO co-immunoprecipitates with SEC24 (binding partner for SEC23) (18), a similar pancreatic phenotype was observed for *Sec23b*$^{gt/gt}$ mice and a second targeted allele. However, to rule out any residual function of the *Sec23b*^{gt} allele masking a hematopoietic phenotype, another set of transplant experiments was performed with FLCs derived from a second *Sec23b* mutant allele, *Sec23b*$^{-}$ (excision of exons 5 and 6 (Fig. 1)), which should result in a protein truncated after amino acid 130 (the full length SEC23B protein contains 767 amino acids).

FLC were harvested from E16.5 *Sec23b*$^{-/-}$ embryos and transplanted into lethally irradiated C57BL/6J recipients ubiquitously expressing GFP (UBC-GFP$^{tg/+}$). Reconstituted hematopoietic cells in recipient mice were GFP(-), confirming donor stem cell engraftment. At 2 months and 5 months post-transplantation, transplant recipients of *Sec23b*$^{-/-}$ FLC exhibited normal RBC counts (Fig. 10A), hemoglobin (Fig. 10B), and hematocrit (Fig. 10C) levels, indistinguishable from recipients of control FLCs. RBC ghosts prepared from reconstituted *Sec23b*$^{-/-}$ peripheral blood demonstrated no evidence of an alteration in band 3 glycosylation compared to control ghosts by western blot (Fig. 10D). Additionally, Ter119+ erythroid precursors isolated from *Sec23b*$^{-/-}$ FLC did not exhibit the “double membrane” appearance on transmission electron microscopy (Fig. 10 E) that is characteristic of human CDAII.

BM SEC23B deficient erythroid cells are normally distributed among stages of erythroid development

Ter119+ erythroid cells were determined by flow cytometry to comprise 37% (standard deviation (SD) = 17%) and 42% (SD = 18%) of the total number of live BM cells in mice transplanted with *Sec23b*$^{-/-}$ and WT FLC, respectively (Fig. 10D). Mice transplanted with *Sec23b*$^{-/-}$ FLC did not exhibit an increase in the percentage of BM bi-/multi-nucleated RBC precursors (Fig. 10E).

To test for stage-specific defects in erythroid maturation resulting from murine SEC23B-deficiency, BM Ter119+ erythroid cells from mice transplanted with either *Sec23b*$^{-/-}$ or WT FLC were stratified by Ter119 expression, CD71 expression, and forward scatter into 5 distinct populations of erythroid development, designated stages I to V (22). Stage I is the earliest stage and consists predominantly of proerythroblasts. Erythroid cells progress through stages I, II, III, and IV in chronological order, and ultimately reach the final stage, stage V, which encompasses primarily mature RBCs.

The distribution of BM erythroid cells among the 5 stages of erythroid development was comparable in mice transplanted with *Sec23b*$^{-/-}$ FLC and control mice transplanted with WT FLC (Fig. 10F).

SEC23A protein level is increased in SEC23B deficient erythroid precursors

Anti-SEC23A and anti-SEC23B anti-peptide antibodies were generated and tested for specificity to their respective paralogs (Fig. 11A and B). SEC23B protein was undetectable by western blot in *Sec23b*$^{-/-}$ FLC and in sorted Ter119+ *Sec23b*$^{-/-}$ erythroid precursors (Fig. 11C and D). *Sec23b* mRNA isolated from *Sec23b*$^{-/-}$ erythroid

342 precursors was markedly reduced, likely due to nonsense mediated decay resulting
343 from the exon 5-6 deletion and resulting frameshift (23) (Fig. 11E). To assess any
344 potential change in SEC23A protein levels in response to loss of SEC23B, quantitative
345 western blot analysis was performed, revealing an ~50% increase in the steady state
346 levels of SEC23A protein in SEC23B-deficient compared to WT erythroid cells (Fig.
347 11F). However, no change In the mRNA expression of the four *Sec24* paralogs, the two
348 *Sar1* paralogs or TRAPPC3 were observed between SEC23B-deficient and WT
349 erythroid cells as measured by qPCR (Fig. 11G).

Discussion

Homozygous or compound heterozygous *SEC23B* mutations in humans result in CDAII, with the clinical phenotype restricted to a characteristic set of RBC abnormalities, and no reported non-hematologic clinical manifestations. In contrast, SEC23B-deficient mice die perinatally, exhibiting degeneration of multiple professional secretory tissues, with apparently normal RBCs. However, the failure of these mice to survive beyond the immediate perinatal period precluded detailed RBC analysis and characterization of adult hematopoiesis. To address this issue, we performed FLC transplantation experiments to generate chimeric mice with SEC23B-deficiency restricted to the hematopoietic compartment. Surprisingly, no RBC abnormalities characteristic of human CDAII could be detected in these animals. In addition to the absence of anemia, SEC23B-deficient RBCs lacked the duplicated membrane and band 3 glycosylation defects that are characteristic of CDAII in humans. Erythroid hyperplasia and multinucleated RBC precursors were also absent from the BM. Competitive transplants and secondary transplant experiments also failed to uncover even a subtle defect in erythropoiesis or reconstitution of myeloid cells and T-lymphocytes. SEC23B deficient B lineage cells appeared under-represented in the BMs of mice transplanted with equal numbers of *Sec23b*$^{gt/gt}$ and WT FLC. However, this finding was not associated with a reduction in the number of SEC23B null B-lymphocytes in the peripheral blood of these chimeric animals, thus its significance remains unclear. Furthermore, secondary recipients of BM harvested from these mice did not exhibit a decreased contribution of the peripheral blood *Sec23b*$^{gt/gt}$ B-lymphocytes compared to their WT counterparts. We confirmed the absence of SEC23B protein in *Sec23b*$^{-/-}$ erythroid precursors, with qPCR

373 analysis of mRNA isolated from *Sec23b*$^{-/-}$ erythroid precursors demonstrating a marked
374 reduction in *Sec23b* mRNA, likely due to nonsense mediated decay (23).

375 SEC23B is ubiquitously expressed in various tissues (18, 24, 25) and is an integral
376 component of COPII vesicles, which facilitate the transport of ~ 8000 proteins from the
377 ER to the Golgi apparatus (26). Despite this broad and fundamental function, SEC23B-
378 deficiency in humans results in a phenotype restricted to the RBC compartment.
379 Though deficiencies of the inner COPII coat components, SEC23, SEC24, and SAR1,
380 are all lethal in yeast, the corresponding COPII proteins for which deficiencies have
381 been reported in mice or humans show a wide range of phenotypes. SEC23A deficiency
382 in humans (discussed below) results in cranio-lenticulo-sutural-dysplasia (15), whereas
383 SEC24A, SEC24B and SEC24D deficiency in mice result in low plasma cholesterol
384 (27), chraniorachischisis (28), and early embryonic lethality (29), respectively. *SAR1B*
385 mutations in humans result in a disease of lipid malabsorption and chylomicron
386 accumulation in the enterocytes (30). It is interesting to note that other genetic
387 deficiencies affecting a large portion of the proteome also selectively disrupt the
388 erythroid compartment, including mutations in genes encoding several ribosomal
389 proteins resulting in Diamond-Blackfan syndrome. These observations suggest that the
390 demanding process of RBC production may be particularly sensitive to perturbations of
391 the basic cell machinery.

392 The mouse is a well established model for the study of human hematopoiesis (31), with
393 numerous gene targeted mice closely recapitulating the eythropoietic phenotypes of the
394 corresponding human diseases (32-36). The lack of conservation in SEC23B deficient

phenotypes between humans and mice is particularly surprising, given the previous report of a CDAII-like phenotype in SEC23B-deficient zebrafish embryos (4).

The mammalian genome encodes 2 *SEC23* paralogues, *SEC23A* and *SEC23B*. In humans, *SEC23A* mutations result in cranio-lenticulo-sutural-dysplasia (15), an autosomal recessive disease thought to result from abnormal collagen secretion. This disease is characterized by skeletal abnormalities, late closure of fontanelles, dysmorphic features, and sutural cataracts. Though SEC23A-deficient mice have not been reported, *Sec23a* deficient zebrafish exhibit abnormal cartilage development reminiscent of the human phenotype (15, 37). The SEC23A and SEC23B proteins exhibit a high degree of sequence similarity (~ 85% identical at the amino acid level), suggesting that the 2 *SEC23* paralogs may overlap extensively in function and that the disparate phenotypes of SEC23B deficiency in humans and mice could be due to a shift in tissue-specific expression patterns during mammalian evolution. Consistent with this hypothesis, recently reported analyses of SEC23A/B in cultured erythroid progenitors (38) and transcriptomes for human and murine erythroid cells at several stages of terminal maturation (39, 40), demonstrate different patterns of SEC23A/SEC23B expression in humans and mice. This is evident particularly in the latest stage of erythroid maturation, with SEC23B the predominant paralog in humans and SEC23A in mice. However, an additional unique function for SEC23B in the human erythroid compartment that is not required in mice, cannot be excluded.

Of note, western blot analysis demonstrates an increase of steady state SEC23A protein levels in SEC23B-deficient erythroid progenitors, suggesting a balance between the SEC23A and B cytoplasmic pools, potentially mediated via SEC23/24 heterodimer

formation. This is similar to the increase in SEC24B observed in hepatocytes of SEC24A deficient mice (27). However, there was no apparent change in the mRNA expression of other core components of the COPII vesicles.

Reports of curative bone marrow transplantation for CDAII (9, 16) indicate that the pathologic defect in this disease is confined to a transplanted cell. However, the mechanism by which human SEC23B-deficiency results in the unique erythropoietic phenotype of CDAII remains unknown. The role of SEC23 in ER-to-Golgi transport suggests that CDAII results from the impaired secretion of one or more key cargo proteins that depend on SEC23B for export from the ER. Mutation of *scl4a1* (the gene encoding band 3) in zebrafish results in increased binucleated erythroblasts, suggesting that band 3 could be the critical cargo, with CDAII resulting from a selective block in its transport to the membrane (41). However, humans with band 3 mutations exhibit hereditary spherocytosis and other RBC shape disorders, but not CDAII (42, 43). The observation that RBCs from CDAII patients are lysed in some but not all acidified normal sera (Ham's test) (1, 2), may provide a clue as to the identity of the critical SEC23B dependent secretory cargo(s).

SEC23B interacts directly with SEC31, a component of the outer layer of the COPII coat. SEC23B also interacts with Bet3 (44), a component of the tethering complex TRAPPI, and with p150Glued (45), a component of the dynactin complex. Whether these direct SEC23B interactions contribute to the pathophysiology of CDAII is unknown.

In conclusion, we have shown that mice with hematopoietic deficiency of SEC23B support a normal erythroid compartment. Future studies aimed at understanding the functional overlap between SEC23A and SEC23B, as well as the specific protein cargos dependent on SEC23A/B for exit from the ER, should provide further insight into the pathophysiology of CDAII.

Acknowledgments

This work was supported by National Institute of Health Grants R01 HL039693 and P01-HL057346 (DG), R01 AI091627 (IM), and R01 HL094505 (BZ). David Ginsburg is a Howard Hughes Medical Institute investigator.

The authors would like to thank Sasha Meshinchi and Jeff Harrison from the Microscopy and Image-Analysis Laboratory at the University of Michigan for help with electron microscopy. The authors would like to acknowledge Elizabeth Hughes, Keith Childs, and Thomas Saunders for preparation of gene targeted mice and the Transgenic Animal Model Core of the University of Michigan's Biomedical Research Core Facilities. Core support was provided by the University of Michigan Cancer Center (P30 CA046592).

Authorship and conflict of interest:

Contribution: RK, MV, and DG conceived the study and designed experiments. RK, MV and MJ performed most of the experiments. BZ, LE, JT, and DS contributed to the execution of the experiments. RK and DG wrote the paper. All authors contributed to the integration and discussion of the results.

Conflict of interest disclosure: The authors declare no competing conflicts of interest.

REFERENCES

1. **Heimpel H, Anselstetter V, Chrobak L, Denecke J, Einsiedler B, Gallmeier K, Griesshammer A, Marquardt T, Janka-Schaub G, Kron M, Kohne E.** 2003. Congenital dyserythropoietic anemia type II: epidemiology, clinical appearance, and prognosis based on long-term observation. Blood **102:**4576-4581.
2. **Khoriaty R, Vasievich MP, Ginsburg D.** 2012. The COPII pathway and hematologic disease. Blood **120:**31-38.
3. **Alloisio N, Texier P, Denoroy L, Berger C, Miraglia del Giudice E, Perrotta S, Iolascon A, Gilsanz F, Berger G, Guichard J.** 1996. The cisternae decorating the red blood cell membrane in congenital dyserythropoietic anemia (type II) originate from the endoplasmic reticulum. Blood **87:**4433-4439.
4. **Schwarz K, Iolascon A, Verissimo F, Trede NS, Horsley W, Chen W, Paw BH, Hopfner KP, Holzmann K, Russo R, Esposito MR, Spano D, De Falco L, Heinrich K, Joggerst B, Rojewski MT, Perrotta S, Denecke J, Pannicke U, Delaunay J, Pepperkok R, Heimpel H.** 2009. Mutations affecting the secretory COPII coat component SEC23B cause congenital dyserythropoietic anemia type II. Nat Genet **41:**936-940.
5. **Zanetti G, Pahuja KB, Studer S, Shim S, Schekman R.** 2012. COPII and the regulation of protein sorting in mammals. Nat Cell Biol **14:**20-28.
6. **Bianchi P, Fermo E, Vercellati C, Boschetti C, Barcellini W, Iurlo A, Marcello AP, Righetti PG, Zanella A.** 2009. Congenital dyserythropoietic anemia type II (CDAII) is caused by mutations in the SEC23B gene. Hum Mutat **30:**1292-1298.
7. **Russo R, Esposito MR, Asci R, Gambale A, Perrotta S, Ramenghi U, Forni GL, Uygun V, Delaunay J, Iolascon A.** Mutational spectrum in congenital dyserythropoietic anemia type II: identification of 19 novel variants in SEC23B gene. Am J Hematol **85:**915-920.
8. **Amir A, Dgany O, Krasnov T, Resnitzky P, Mor-Cohen R, Bennett M, Berrebi A, Tamary H.** 2011. E109K is a SEC23B founder mutation among Israeli Moroccan Jewish patients with congenital dyserythropoietic anemia type II. Acta haematologica **125:**202-207.
9. **Fermo E, Bianchi P, Notarangelo LD, Binda S, Vercellati C, Marcello AP, Boschetti C, Barcellini W, Zanella A.** CDAII presenting as hydrops foetalis: molecular characterization of two cases. Blood Cells Mol Dis **45:**20-22.
10. **Iolascon A, Russo R, Esposito MR, Asci R, Piscopo C, Perrotta S, Feneant-Thibault M, Garcon L, Delaunay J.** 2010. Molecular analysis of 42 patients with congenital dyserythropoietic anemia type II: new mutations in the SEC23B gene and a search for a genotype-phenotype relationship. Haematologica **95:**708-715.
11. **Punzo F, Bertoli-Avella AM, Scianguetta S, Della Ragione F, Casale M, Ronzoni L, Cappellini MD, Forni G, Oostra BA, Perrotta S.** 2011. Congenital dyserythropoietic anemia type II: molecular analysis and expression of the SEC23B gene. Orphanet journal of rare diseases **6:**89.
12. **Russo R, Gambale A, Esposito MR, Serra ML, Troiano A, De Maggio I, Capasso M, Luzzatto L, Delaunay J, Tamary H, Iolascon A.** 2011. Two founder mutations in the SEC23B gene account for the relatively high frequency of CDA II in the Italian population. Am J Hematol **86:**727-732.
13. **Liu G, Niu S, Dong A, Cai H, Anderson GJ, Han B, Nie G.** 2012. A Chinese family carrying novel mutations in SEC23B and HFE2, the genes responsible for congenital dyserythropoietic anaemia II (CDA II) and primary iron overload, respectively. Br J Haematol **158:**143-145.
14. **Russo R, Langella C, Esposito MR, Gambale A, Vitiello F, Vallefuoco F, Ek T, Yang E, Iolascon A.** 2013. Hypomorphic mutations of SEC23B gene account for mild phenotypes of congenital dyserythropoietic anemia type II. Blood Cells Mol Dis **51:**17-21.

15. **Boyadjiev SA, Fromme JC, Ben J, Chong SS, Nauta C, Hur DJ, Zhang G, Hamamoto S, Schekman R, Ravazzola M, Orci L, Eyaid W.** 2006. Cranio-lenticulo-sutural dysplasia is caused by a SEC23A mutation leading to abnormal endoplasmic-reticulum-to-Golgi trafficking. Nat Genet **38:**1192-1197.
16. **Iolascon A, Sabato V, de Mattia D, Locatelli F.** 2001. Bone marrow transplantation in a case of severe, type II congenital dyserythropoietic anaemia (CDA II). Bone Marrow Transplant **27:**213-215.
17. **Remacha AF, Badell I, Pujol-Moix N, Parra J, Muniz-Diaz E, Ginovart G, Sarda MP, Hernandez A, Moliner E, Torrent M.** 2002. Hydrops fetalis-associated congenital dyserythropoietic anemia treated with intrauterine transfusions and bone marrow transplantation. Blood **100:**356-358.
18. **Tao J, Zhu M, Wang H, Afelik S, Vasievich MP, Chen XW, Zhu G, Jensen J, Ginsburg D, Zhang B.** 2012. SEC23B is required for the maintenance of murine professional secretory tissues. Proc Natl Acad Sci U S A **109:**E2001-2009.
19. **Schaefer BC, Schaefer ML, Kappler JW, Marrack P, Kedl RM.** 2001. Observation of antigen-dependent CD8+ T-cell/ dendritic cell interactions in vivo. Cell Immunol **214:**110-122.
20. **Kiel MJ, Yilmaz OH, Iwashita T, Yilmaz OH, Terhorst C, Morrison SJ.** 2005. SLAM family receptors distinguish hematopoietic stem and progenitor cells and reveal endothelial niches for stem cells. Cell **121:**1109-1121.
21. **Chen ML, Logan TD, Hochberg ML, Shelat SG, Yu X, Wilding GE, Tan W, Kujoth GC, Prolla TA, Selak MA, Kundu M, Carroll M, Thompson JE.** 2009. Erythroid dysplasia, megaloblastic anemia, and impaired lymphopoiesis arising from mitochondrial dysfunction. Blood **114:**4045-4053.
22. **Chen K, Liu J, Heck S, Chasis JA, An X, Mohandas N.** 2009. Resolving the distinct stages in erythroid differentiation based on dynamic changes in membrane protein expression during erythropoiesis. Proc Natl Acad Sci U S A **106:**17413-17418.
23. **Losson R, Lacroute F.** 1979. Interference of nonsense mutations with eukaryotic messenger RNA stability. Proc Natl Acad Sci U S A **76:**5134-5137.
24. **Fromme JC, Ravazzola M, Hamamoto S, Al-Balwi M, Eyaid W, Boyadjiev SA, Cosson P, Schekman R, Orci L.** 2007. The genetic basis of a craniofacial disease provides insight into COPII coat assembly. Dev Cell **13:**623-634.
25. **Paccaud JP, Reith W, Carpentier JL, Ravazzola M, Amherdt M, Schekman R, Orci L.** 1996. Cloning and functional characterization of mammalian homologues of the COPII component Sec23. Mol Biol Cell **7:**1535-1546.
26. **Kanapin A, Batalov S, Davis MJ, Gough J, Grimmond S, Kawaji H, Magrane M, Matsuda H, Schonbach C, Teasdale RD, Yuan Z.** 2003. Mouse proteome analysis. Genome Res **13:**1335-1344.
27. **Chen XW, Wang H, Bajaj K, Zhang P, Meng ZX, Ma D, Bai Y, Liu HH, Adams E, Baines A, Yu G, Sartor MA, Zhang B, Yi Z, Lin J, Young SG, Schekman R, Ginsburg D.** 2013. SEC24A deficiency lowers plasma cholesterol through reduced PCSK9 secretion. eLife **2:**e00444.
28. **Merte J, Jensen D, Wright K, Sarsfield S, Wang Y, Schekman R, Ginty DD.** Sec24b selectively sorts Vangl2 to regulate planar cell polarity during neural tube closure. Nat Cell Biol **12:**41-46; sup pp 41-48.
29. **Baines AC, Adams EJ, Zhang B, Ginsburg D.** 2013. Disruption of the Sec24d gene results in early embryonic lethality in the mouse. PLoS One **8:**e61114.
30. **Jones B, Jones EL, Bonney SA, Patel HN, Mensenkamp AR, Eichenbaum-Voline S, Rudling M, Myrdal U, Annesi G, Naik S, Meadows N, Quattrone A, Islam SA, Naoumova RP, Angelin B, Infante R, Levy E, Roy CC, Freemont PS, Scott J, Shoulders CC.** 2003. Mutations in a Sar1 GTPase of COPII vesicles are associated with lipid absorption disorders. Nat Genet **34:**29-31.

31. **Orkin SH, Zon LI.** 2008. Hematopoiesis: an evolving paradigm for stem cell biology. Cell **132:**631-644.
32. **White RA, Birkenmeier CS, Lux SE, Barker JE.** 1990. Ankyrin and the hemolytic anemia mutation, nb, map to mouse chromosome 8: presence of the nb allele is associated with a truncated erythrocyte ankyrin. Proc Natl Acad Sci U S A **87:**3117-3121.
33. **Bodine DMt, Birkenmeier CS, Barker JE.** 1984. Spectrin deficient inherited hemolytic anemias in the mouse: characterization by spectrin synthesis and mRNA activity in reticulocytes. Cell **37:**721-729.
34. **Hughes MR, Anderson N, Maltby S, Wong J, Berberovic Z, Birkenmeier CS, Haddon DJ, Garcha K, Flenniken A, Osborne LR, Adamson SL, Rossant J, Peters LL, Minden MD, Paulson RF, Wang C, Barber DL, McNagny KM, Stanford WL.** 2011. A novel ENU-generated truncation mutation lacking the spectrin-binding and C-terminal regulatory domains of Ank1 models severe hemolytic hereditary spherocytosis. Experimental hematology **39:**305-320, 320 e301-302.
35. **Siatecka M, Sahr KE, Andersen SG, Mezei M, Bieker JJ, Peters LL.** 2010. Severe anemia in the Nan mutant mouse caused by sequence-selective disruption of erythroid Kruppel-like factor. Proc Natl Acad Sci U S A **107:**15151-15156.
36. **Finberg KE, Heeney MM, Campagna DR, Aydinok Y, Pearson HA, Hartman KR, Mayo MM, Samuel SM, Strouse JJ, Markianos K, Andrews NC, Fleming MD.** 2008. Mutations in TMPRSS6 cause iron-refractory iron deficiency anemia (IRIDA). Nat Genet **40:**569-571.
37. **Lang MR, Lapierre LA, Frotscher M, Goldenring JR, Knapik EW.** 2006. Secretory COPII coat component Sec23a is essential for craniofacial chondrocyte maturation. Nat Genet **38:**1198-1203.
38. **Satchwell TJ, Pellegrin S, Bianchi P, Hawley BR, Gampel A, Mordue KE, Budnik A, Fermo E, Barcellini W, Stephens DJ, van den Akker E, Toye AM.** 2013. Characteristic phenotypes associated with congenital dyserythropoietic anemia (type II) manifest at different stages of erythropoiesis. Haematologica **98:**1788-1796.
39. **An X, Schulz VP, Li J, Wu K, Liu J, Xue F, Hu J, Mohandas N, Gallagher PG.** 2014. Global transcriptome analyses of human and murine terminal erythroid differentiation. Blood **123:**3466-3477.
40. **Pishesha N, Thiru P, Shi J, Eng JC, Sankaran VG, Lodish HF.** 2014. Transcriptional divergence and conservation of human and mouse erythropoiesis. Proc Natl Acad Sci U S A **111:**4103-4108.
41. **Paw BH, Davidson AJ, Zhou Y, Li R, Pratt SJ, Lee C, Trede NS, Brownlie A, Donovan A, Liao EC, Ziai JM, Drejer AH, Guo W, Kim CH, Gwynn B, Peters LL, Chernova MN, Alper SL, Zapata A, Wickramasinghe SN, Lee MJ, Lux SE, Fritz A, Postlethwait JH, Zon LI.** 2003. Cell-specific mitotic defect and dyserythropoiesis associated with erythroid band 3 deficiency. Nat Genet **34:**59-64.
42. **Grace RF, Lux SE.** 2009. Disorders of the red cell membrane., p. 659-837. *In* Orkin SH, Nathan DG, Ginsburg D, Look AT, Fisher DE, Lux E (ed.), Hematology of infancy and childhood. Saunders, Philadelphia, PA.
43. **Iolascon A, De Falco L, Borgese F, Esposito MR, Avvisati RA, Izzo P, Piscopo C, Guizouarn H, Biondani A, Pantaleo A, De Franceschi L.** 2009. A novel erythroid anion exchange variant (Gly796Arg) of hereditary stomatocytosis associated with dyserythropoiesis. Haematologica **94:**1049-1059.
44. **Cai H, Yu S, Menon S, Cai Y, Lazarova D, Fu C, Reinisch K, Hay JC, Ferro-Novick S.** 2007. TRAPPI tethers COPII vesicles by binding the coat subunit Sec23. Nature **445:**941-944.
45. **Watson P, Forster R, Palmer KJ, Pepperkok R, Stephens DJ.** 2005. Coupling of ER exit to microtubules through direct interaction of COPII with dynactin. Nat Cell Biol **7:**48-55.

602 **Figure Legends:**

603 **Figure 1. *Sec23b* mutant alleles.** (A) Schematic of the first *Sec23b* gene-trap allele
604 demonstrating a gene-trap insertion into intron 19.(18) SA, splice acceptor cassette; β-
605 Geo, β-galactosidase-neo fusion; pA, poly-adenylation sequence. (B) The *Sec23b*
606 conditional gene-trap allele (*Sec23b*^{cgt}) contains a gene trap insertion in intron 4 flanked
607 by 2 FRT sites. Mice carrying this allele were crossed to β-actin FLP transgenic mice.
608 Mice heterozygous for the resulting *Sec23b* floxed allele (*Sec23b*$^{+/fl}$) were crossed to
609 EIIACre transgenic mice to excise exons 5 and 6, and generate the *Sec23b* null allele
610 (*Sec23b*$^{-}$). Gray boxes represent exons with exon number indicated in the box. F1, F2,
611 R1, cgtB1, and cgtR1 represent *Sec23b* genotyping primers. En2 SA, splice acceptor of
612 mouse *En2* exon 2; IRES, encephalomyocarditis virus internal ribosomal entry site;
613 *lacZ*, *E.coli* β-galactosidase gene; pA, SV40 plyadenylation signal; *βact:neo*, human β-
614 actin promoter-driven neomycin cassette. (C) A three-primer PCR assay (F1, cgtB1,
615 cgtR1) distinguishes the *Sec23b*^{cgt} allele (F1:cgtB1, 344 bp) and the WT allele
616 (F1:cgtR1, 475 bp). (D) A three-primer PCR assay (F1, F2, R1) distinguishes the
617 alleles: *Sec23b*$^{+}$ (F2:R1, 235 bp), *Sec23b*^{fl} (F2:R1, 269 bp), and *Sec23b*$^{-}$ (F1:R1, 336
618 bp). Location of the primers are indicated in Figures 1A and 1B. The gene structures
619 depicted in figures 1A and 1B are not according to scale.

620 **Figure 2. FACS analysis of E17.5 *Sec23b*$^{gt/gt}$ and WT FLC.** (A) Livers were harvested
621 from 3 *Sec23b*$^{gt/gt}$ and 3 WT E17.5 embryos. Flow cytometry on FLC single cell
622 suspensions demonstrated equivalent total number of recovered cells from *Sec23b*$^{gt/gt}$
623 and WT fetal livers. Each liver is represented by 1 point, and horizontal lines indicate
624 mean value for each group. (B) The number of long-term hematopoietic stem cells (ckit+

Sca1+ CD48- CD150+ Lin-) was equivalent for *Sec23b*$^{gt/gt}$ and WT fetal livers. (C) FACS distributions for cell sorts used to calculate long-term hematopoietic stem cells in B.

Figure 3. Transplant recipients of *Sec23b*$^{gt/gt}$ FLC do not exhibit CDAII. Mice transplanted with *Sec23b*$^{gt/gt}$ FLC demonstrated equivalent (A) hemoglobin and (B) hematocrit levels as compared to mice transplanted with control WT FLC over the course of 25 weeks of post-transplantation follow-up ($p > 0.05$ for all time points). N = 5-7 mice per group. Error bars represent standard deviation. (C) Spleens harvested from transplant recipients of *Sec23b*$^{gt/gt}$ and WT FLC were equivalent in weights. Recipients of *Sec23b*$^{gt/gt}$ FLC exhibited equivalent (D) myeloid : erythroid ratios and (E) number of bi/multi-nucleated RBC precursors (evaluated independently by two investigators) compared to control mice transplanted with WT FLC. Each dot represents results from one mouse. Horizontal lines indicate means and error bars indicate standard deviation.

Figure 4. RBC from mice transplanted with *Sec23b*$^{gt/gt}$ FLC do not exhibit a band 3 glycosylation defect or a double RBC membrane. (A) RBC ghosts were isolated from *Sec23b*$^{gt/gt}$ and WT RBC and fractionated on sodium dodecylsulfate-polyacrylamide gel electrophoresis. Coomassie blue stain revealed no difference in the appearance of the RBC membrane protein band 3 in *Sec23b*$^{gt/gt}$ RBC ghosts. Each lane represents a sample from a different individual mouse. (B) Similarly, band 3 protein appeared indistinguishable on western blotting bteween *Sec23b*$^{gt/gt}$ and WT RBC ghosts. (C) *Sec23b*$^{gt/gt}$ RBC lack the “double membrane” appearance on transmission electron microscopy characteristic of human CDAII. RBC were evaluated at three different magnifications, illustrated in the right lower corner of each figure. Arrows indicate RBC membrane.

Figure 5. *Sec23b*$^{gt/gt}$ FLC do not exhibit a competitive disadvantage at reconstituting erythropoiesis compared to WT FLC. C57BL/6J mice were co-transplanted with a 1:1 mix of GFP(-) *Sec23b*$^{gt/gt}$ FLC and UBC-GFP^{Tg+} *Sec23b*$^{+/+}$ FLC in a competitive transplant assay (experimental arm). Following engraftment, the percent of GFP(-) cells in the peripheral blood/BM of recipient mice indicate the percent of cells derived from *Sec23b*$^{gt/gt}$ FLC. Control mice were co-transplanted with a 1:1 mix of WT GFP(-) and GFP^{Tg+} *Sec23b*$^{+/+}$ FLC. (A) By peripheral blood FACS, Ter119+ RBC were determined to be derived from both *Sec23b*$^{gt/gt}$ and WT FLC. *Sec23b*$^{gt/gt}$ RBC persisted at a stable level throughout the 18-weeks follow-up period, suggesting no competitive advantage to WT FLC compared to *Sec23b*$^{gt/gt}$ FLC at reconstituting erythropoiesis. (B) In the BM, the contribution of GFP(-) *Sec23b*$^{gt/gt}$ cells to the populations of Ter119+ erythroid precursors was equivalent to the contribution of the GFP(-) WT cells in the control arm. Erythroid cells were further stratified by forward scatter and CD71 expression to identify more primitive progenitors as larger cells expressing higher levels of CD71, more mature smaller cells with lower expression of CD71, and intermediate cells. *Sec23b*$^{gt/gt}$ cells contributed to all subsets of erythroid cells.

Figure 6. Analysis of peripheral blood and BM hematopoietic compartments of mice co-transplanted with a 1:1 mix of GFP(-) *Sec23b*$^{gt/gt}$ FLC and UBC-GFP^{Tg+} *Sec23b*$^{+/+}$ FLC (experimental arm) and control mice co-transplanted with a 1:1 mix of GFP(-) and GFP^{Tg+} *Sec23b*$^{+/+}$ FLC. By peripheral blood FACS, (A) Mac1+ Gr1+ neutrophils, (B) B220+ B-lymphocytes, and (C) CD3+ T-lymphocytes were found to be derived from both *Sec23b*$^{gt/gt}$ and WT FLC. The *Sec23b*$^{gt/gt}$ peripheral blood cells

persisted at a stable level throughout the 18-week follow-up period, suggesting no competitive advantage to WT FLC compared to *Sec23b*$^{gt/gt}$ FLC at reconstituting hematopoiesis. In the BM, the contribution of GFP(-) *Sec23b*$^{gt/gt}$ FLC to (D) the long-term hematopoietic stem cells (ckit+ Sca1+ CD48- CD150- Lin-), and to (E) myeloid cells (Mac1+ GR1+) in the experimental arm was equivalent to the contribution of the GFP(-) WT cells in the control arm. (F) Similarly, the contribution of GFP(-) *Sec23b*$^{gt/gt}$ T-lymphocytes in the thymus was equivalent to that of GFP(-) WT cells in the control arm. *There was a trend for some subsets of GFP(-) *Sec23b*$^{gt/gt}$ T-lymphocytes to be under-represented; however this did not reach statistical significance after correction for multiple observations using the Holm-Sidak method or the Bonferroni method. ISP, immature single positive cells; DP, CD4+ CD8+ double positive T-lymphocytes; NS, not significant. (G) In contrast, GFP(-) *Sec23b*$^{gt/gt}$ CD19+ CD220+ BM B-lymphocytes were under-represented. Each point represents one mouse. Lines represent mean values for each group and error bars indicate standard deviation.

Figure 7. Reconstituted GFP(-) hematopoietic cells in mice co-transplanted with a 1:1 mix of GFP(-) *Sec23b*$^{gt/gt}$ FLC and UBC-GFP^{Tg+} *Sec23b*$^{+/+}$ FLC were derived from *Sec23b*$^{gt/gt}$ FLC and not from host reconstitution. GFP(-) myeloid cells isolated from mice transplanted with a 1:1 ratio of UBC-GFP$^{tg/+}$ FLC and *Sec23b*$^{gt/gt}$ FLC and from control mice transplanted with 1:1 ratio of UBC-GFP$^{tg/+}$ FLC and WT FLC were genotyped for *Sec23b*$^{gt/gt}$. Six mice from each group were examined. Each lane represents the genotype of myeloid cells isolated from a single mouse. Genotype of a *Sec23b*$^{+/gt}$ control DNA is shown. The lower and upper bands correspond to the expected PCR products for the *Sec23b* WT and gt alleles, respectively.

Figure 8. Secondary bone marrow transplantation experiments demonstrate continued equivalence of *Sec23b*$^{gt/gt}$ and WT FLC at reconstituting erythropoiesis. BMs harvested from mice chimeric for GFP(-) *Sec23b*$^{gt/gt}$ and GFP(+) WT hematopoietic cells were transplanted into lethally irradiated secondary recipients (experimental arm). Control mice were transplanted with BMs harvested from mice chimeric for GFP(-) and GFP(+) WT hematopoietic cells. (A) By peripheral blood FACS, the contribution of *Sec23b*$^{gt/gt}$ GFP(-) cells to the population of Ter119+ RBC in the experimental arm was equivalent to the contribution of WT GFP(-) cells in control mice over the course of 18 weeks of follow-up. Peripheral blood analysis was performed on N = 13-15 mice per group. Error bars represent standard deviation. Bone marrow cells were isolated from both hind limbs of each secondary transplant recipient mouse. The contribution of *Sec23b*$^{gt/gt}$ GFP(-) (B) Ter119+ erythroid cells at various stages of differentiation and (C) hematopoietic stem cells (ckit+ Sca1+ CD48- CD150- Lin-) in the experimental mice was equivalent to the contribution of WT GFP(-) cells in the control arm. Each point represents one mouse. Lines represent mean values for each group. P values were calculated by Student's t-test.

Figure 9. Secondary bone marrow transplantation experiments demonstrate continued equivalence of *Sec23b*$^{gt/gt}$ and WT FLC at reconstituting hematopoiesis. BMs harvested from mice chimeric for GFP(-) *Sec23b*$^{gt/gt}$ and GFP(+) WT hematopoietic cells were transplanted into lethally irradiated secondary recipients (experimental arm). Control mice were transplanted with BMs harvested from mice chimeric for GFP(-) and GFP(+) WT hematopoietic cells. Peripheral blood was obtained from recipient mice. By FACS, the contribution of *Sec23b*$^{gt/gt}$ GFP(-) cells to the

population of (A) Mac1+ Gr1+ neutrophils, (B) B220+ B-lymphocytes, and (C) CD3+ T-lymphocytes in the experimental arm was equivalent to the contribution of WT GFP(-) cells in control mice over the course of 18 weeks of follow-up. n = 13-15 mice per group. Error bars represent standard deviation.

Figure 10. Mice transplanted with *Sec23b*$^{-/-}$ FLC do not exhibit an erythroid phenotype. Lethally irradiated UBC-GFP$^{tg/+}$ mice were transplanted with GFP(-) FLC harvested from either *Sec23b*$^{-/-}$ or WT E.16.5 embryos. Reconstituted hematopoietic cells in recipient mice were GFP(-), confirming donor engraftment. Recipients of *Sec23b*$^{-/-}$ FLC had indistinguishable (A) RBC counts, (B) hemoglobin, and (C) hematocrit levels as compared to control recipients of WT FLC. (D) *Sec23b*$^{-/-}$ RBC ghosts did not exhibit a band 3 glycosylation defect by western blot, (E) nor did Ter119+ erythroid precursors demonstrate a "double membrane" by transmission electron microscopy. (F) By FACS analysis, Ter119+ erythroid cells comprised 36.67% (± 16.69 SD) and 41.56% (± 17.68 SD) of total live BM cells harvested from mice transplanted with *Sec23b*$^{-/-}$ and WT FLC, respectively. (G) Mice transplanted with *Sec23b*$^{-/-}$ FLC did not exhibit an increase in the percent of bi/multi-nucleated RBC precursors. (H) BM erythroid compartments were stratified by forward scatter and CD71 expression into 5 stages of erythroid development (stages I through V in chronological order) (22). The distribution of erythroid cells among stages I through V was comparable in mice transplanted with *Sec23b*$^{-/-}$ FLC and mice transplanted with WT FLC. Error bars indicate standard deviation. Means and standard deviation are indicated by horizontal lines.

Figure 11. SEC23A protein level is increased in *Sec23b*$^{-/-}$ erythroid precursors. Lysates from COS cells transfected with GFP-tagged SEC23A or SEC23B were

examined by immunoblotting with antipeptide antibodies raised against (A) SEC23A or (B) SEC23B, demonstrating a high degree of specificity of these antibodies for their respective paralogs. Western blotting of whole cell lysates from (C) WT control and *Sec23b*$^{-/-}$ FLC and (D) sorted control and *Sec23b*$^{-/-}$ Ter119+ erythroid precursors demonstrated no detectable SEC23B protein in *Sec23b*$^{-/-}$ cells. (E) qPCR analysis showed a marked reduction of *Sec23b* mRNA in *Sec23b*$^{-/-}$ compared to WT Ter119+ cells. (F) SEC23A protein level normalized to β-actin or to RalA was increased in Ter119+ erythroid precursors compared to WT controls, as determined by quantitative western blot analysis ($p = 0.029$ and 0.030 for normalization to β-actin and RalA respectively). (G) mRNA levels measured by qPCR for the four Sec24 paralogs, the two Sar1 paralogs, and TRAPPC3 were all indistinguishable between *Sec23b*$^{-/-}$ and WT Ter119+ erythroid cells.

Primer sequences	
Primer	5' → 3' Sequence
Sec23b F1	ATAGACCAGGCTGGCCTCAGTC
Sec23b cgt B1	CCACAACGGGTTCTTCTGTT
Sec23b cgt R1	CGAGCACAGAGAGACCCAAT
Sec23b R	CAAGTGAGTGCCTCCTCACA
Sec23b F2	AACAGCCCAGGTGACTAGGA
Sec23b qPCR F	CCCTACGTCTTTCAGATTGTCA
Sec23b qPCR R	CGGGCAAAATGGTGTCTATAA
Sec24a qPCR F	GAGCAGAGATGGAGCGTTCCT
Sec24a qPCR R	TTCTTCCAACCCAAAGCATCA
Sec24b qPCR F	GACCCGAGAAGGCGCTTT
Sec24b qPCR R	TTTGCCAACCCAAATGTAGAAA
Sec24c qPCR F	TTATGCGGGTTCGGACAAG
Sec24c qPCR R	CTCATATAGAAAGCGCCAAAGAAAT
Sec24d qPCR F	CTCATATAGAAAGCGCCAAAGAAAT
Sec24d qPCR R	TCATGTACACAGGCAGCACCTT
Sar1a qPCR F	TCGGTGGGCATGAGCAA
Sar1a qPCR R	GCCATTAATCGCTGGGAGATAA
Sar1b qPCR F	GGGTGGGCACGTGCAA
Sar1b qPCR R	TGCCATTGATAGCAGGAAGGT
TRAPPC3 qPCR F	GCACGGAGAGCAAGAAAATGA
TRAPPC3 qPCR R	GGTGACAAGCGCTCCATAGG
beta-actin qPCR F	GATCTGGCACCACACCTTCT
beta-actin qPCR R	GGGGTGTTGAAGGTCTCAAA
GAPDH qPCR F	TGTGTCCGTCGTGGATCTGA
GAPDH qPCR R	ACCACCTTCTTGATGTCATCATACTT

Table 1. Genotyping and qPCR primer sequences.

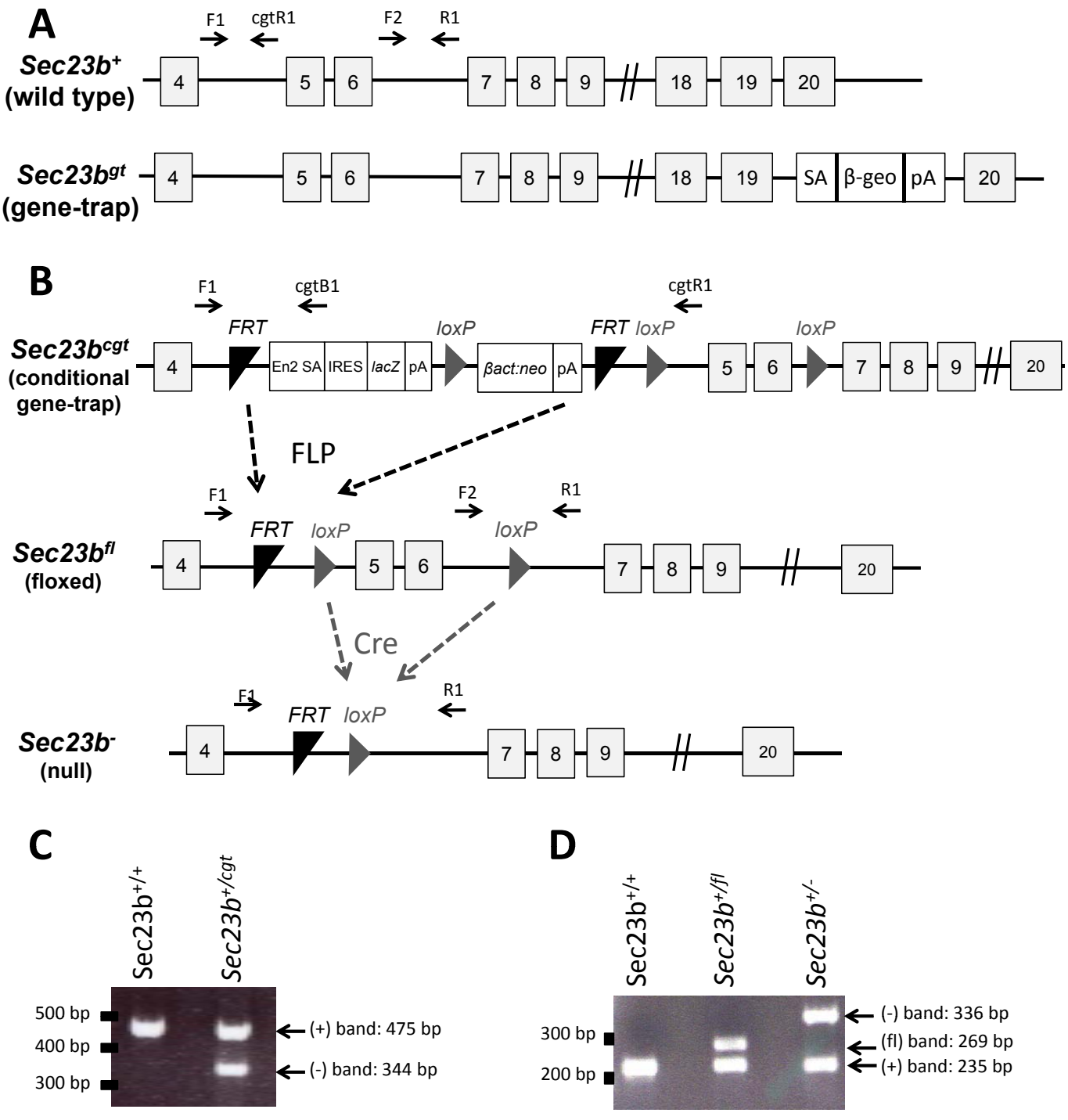

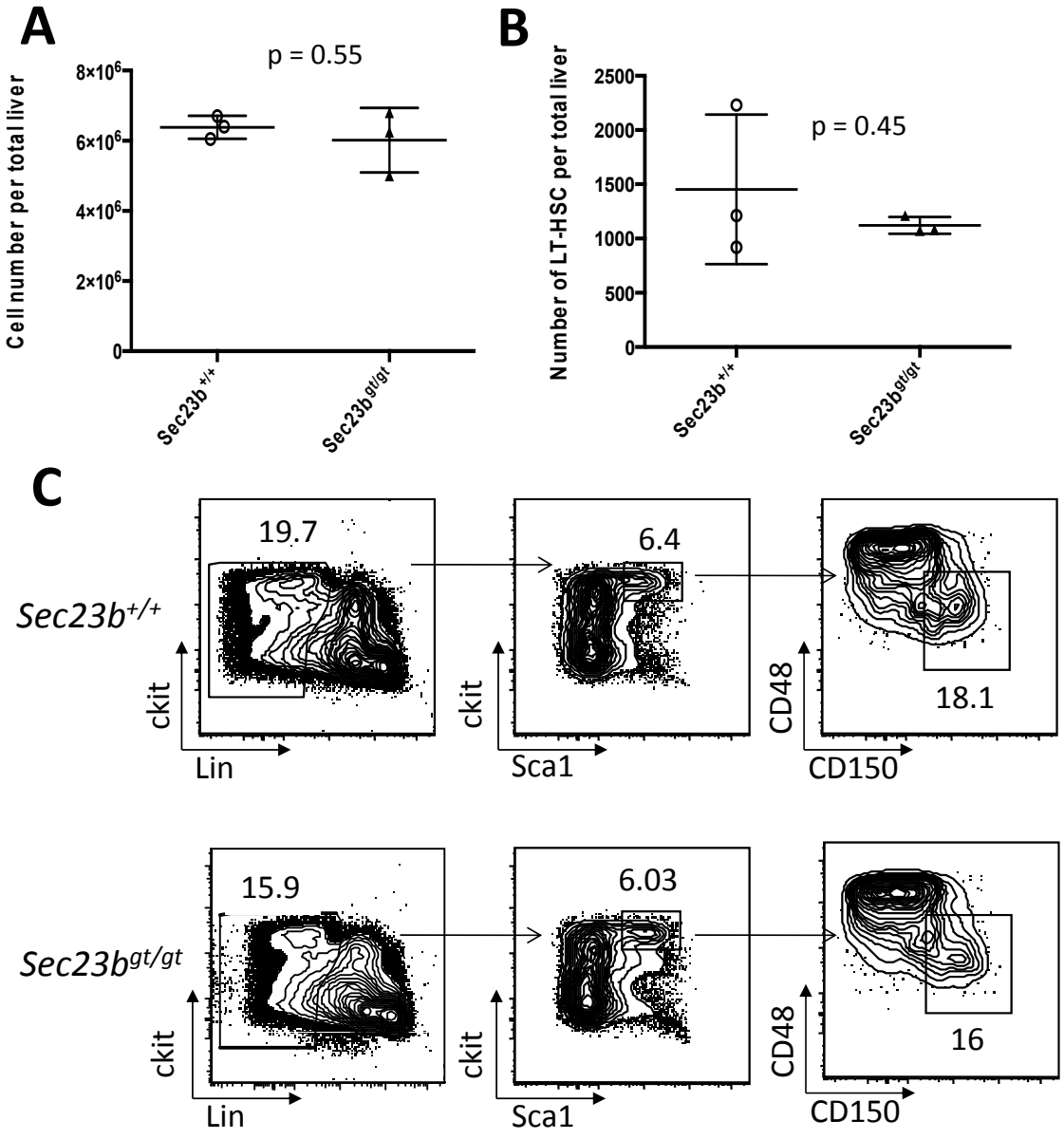

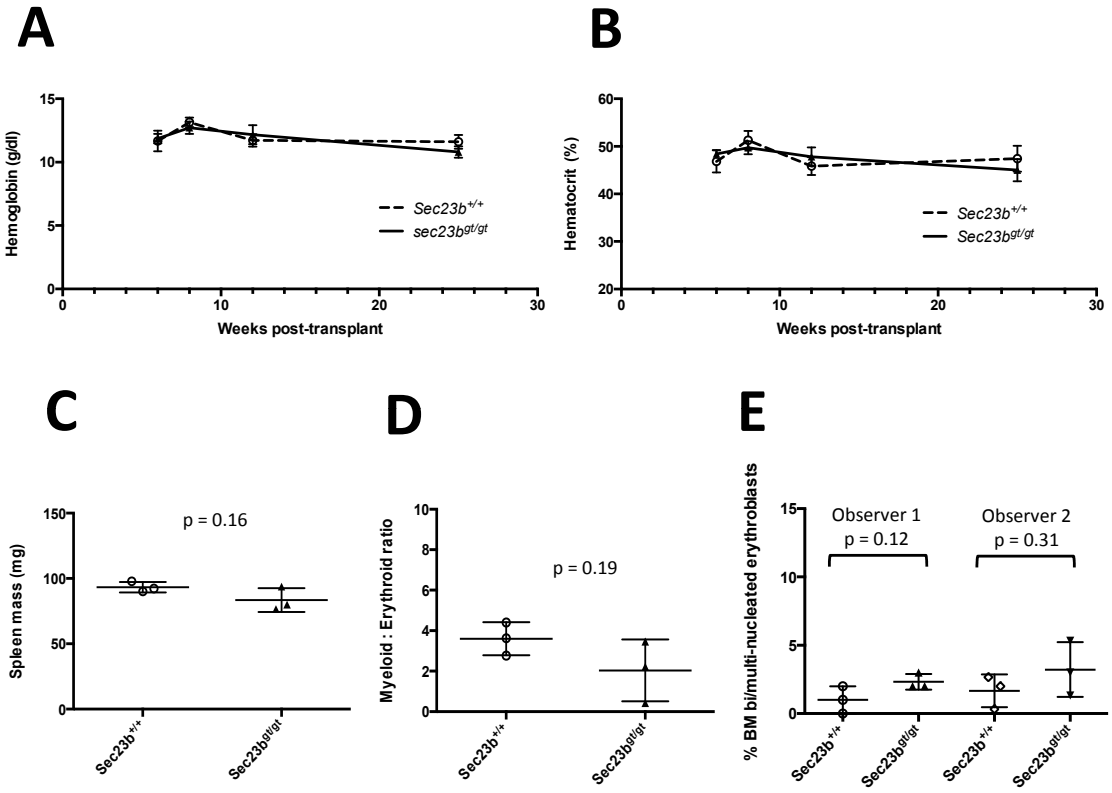

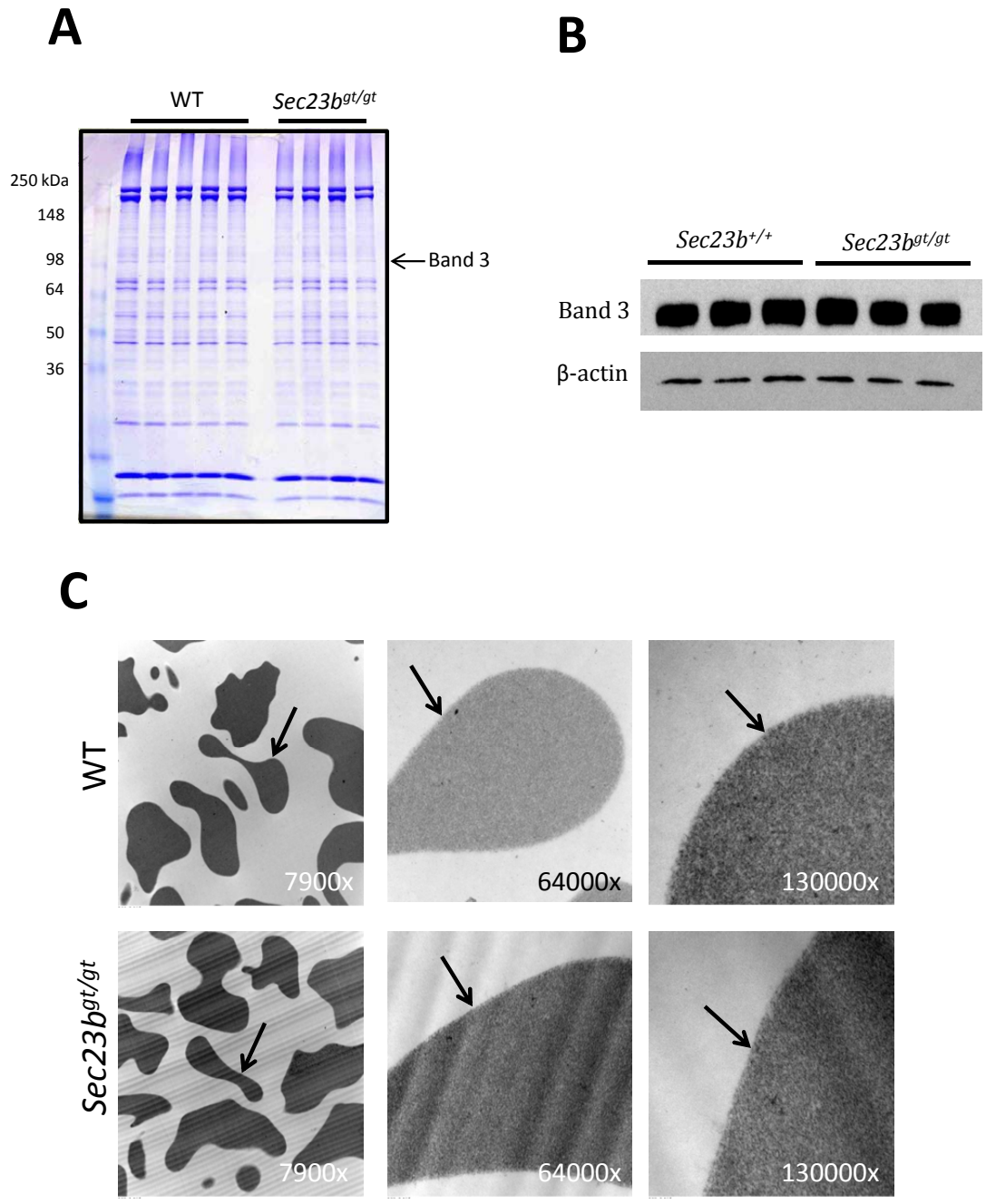

A

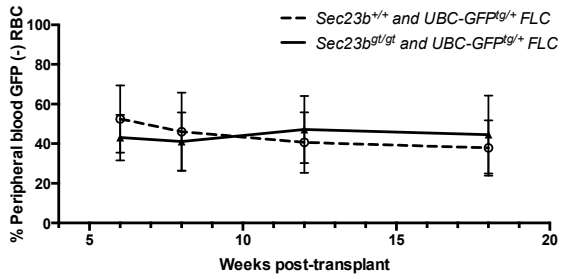

B

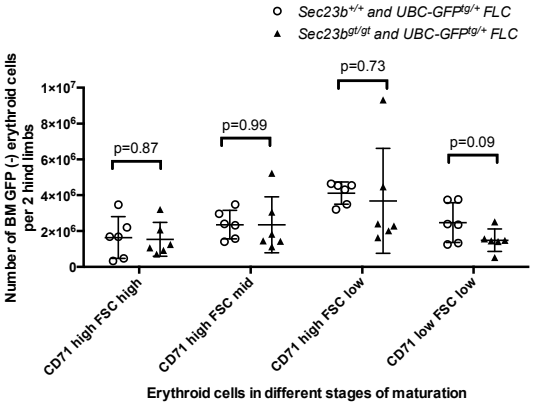

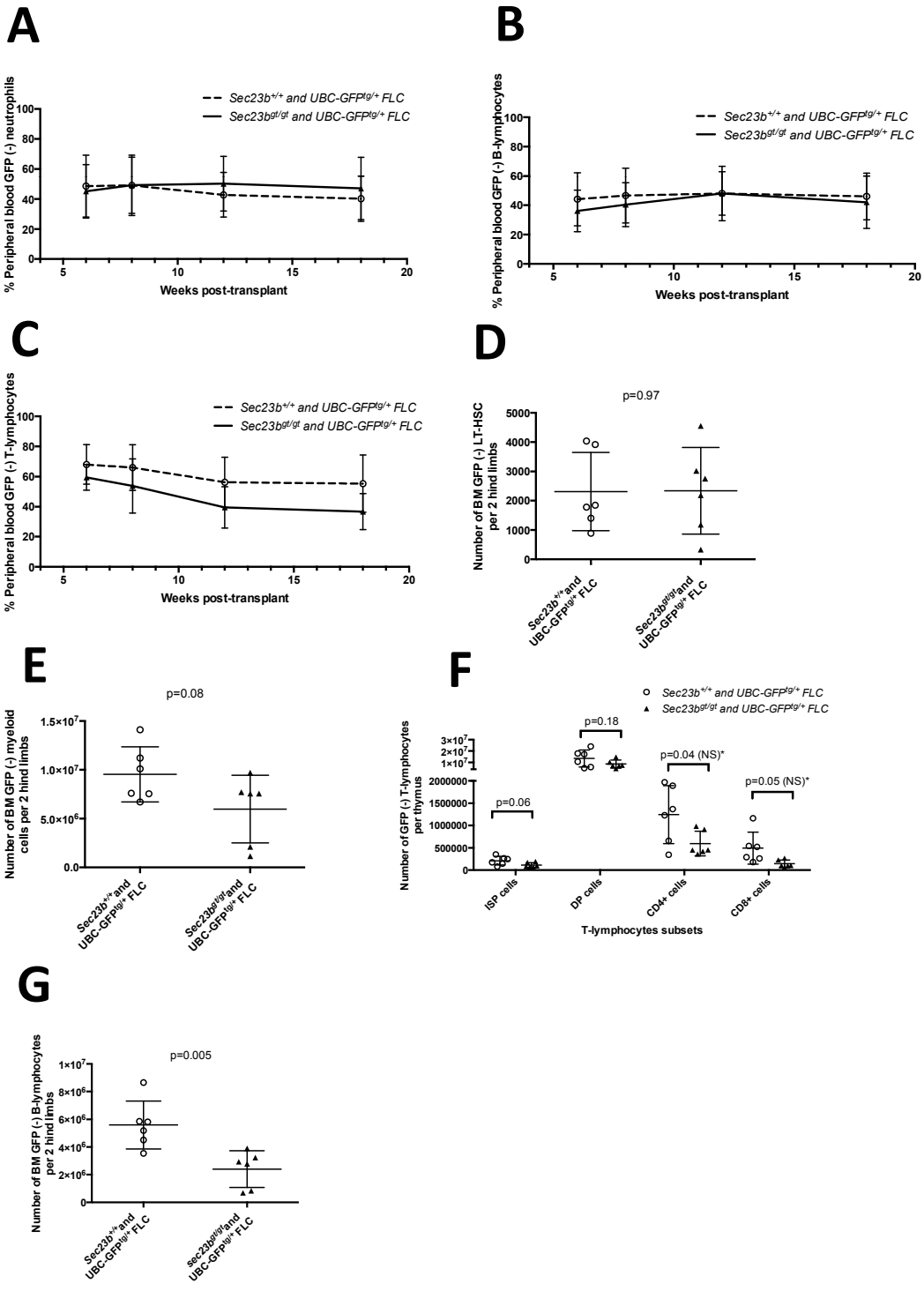

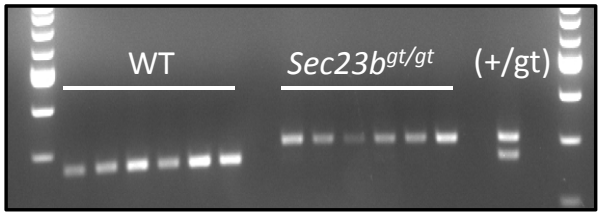

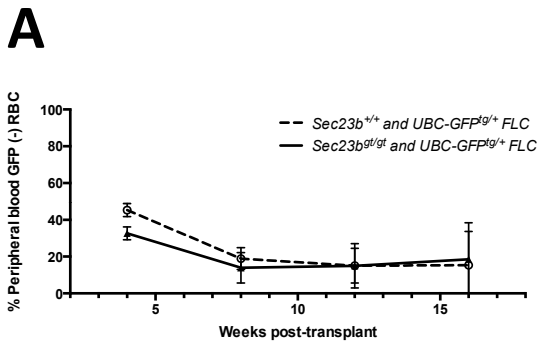

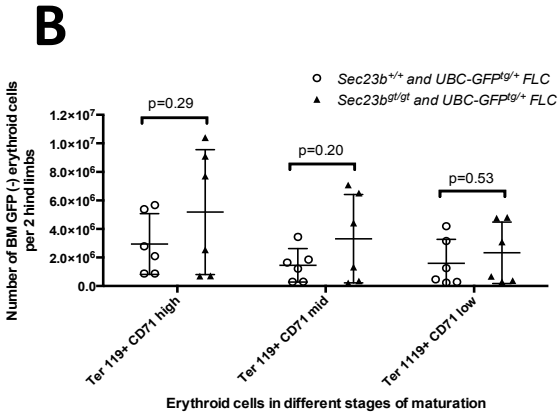

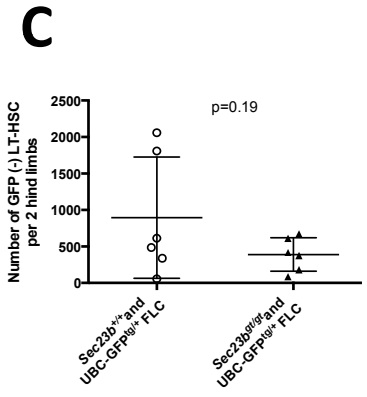

A

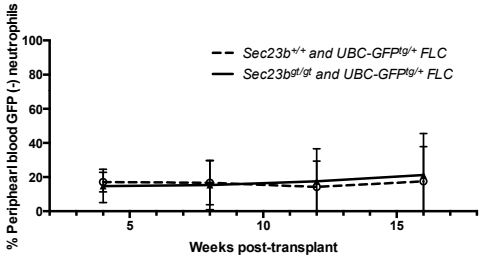

B

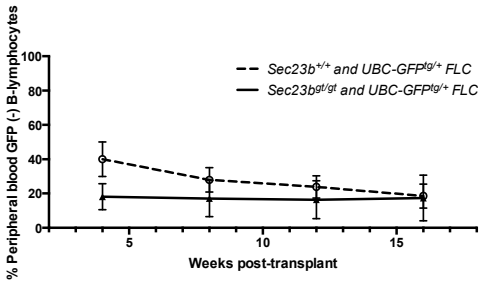

C